DOI: 10.24352/UB.OVGU-2017-095 TECHNISCHE MECHANIK, 37, 2-5, (2017), 181 – 195
submitted: April 12, 2017

Dynamic Behaviour of EHD-contacts using a regularised, mass conserving Cavitation Algorithm

S. Nitzschke, E. Woschke, C. Daniel

The paper deals with the holistic simulation of systems supported in journal bearings, which is demonstrated using the example of a conrod's big end bearing. For that purpose, primarily the interactions of multibody-, structure- and hydrodynamics have to be described. Based on the time integration of the global equations of motions, the non-linear bearing forces in the fluid film and the elastic deformation of the bearings surfaces have to be modelled adequately concerning their mutual influence. The implementation of the elastic structure is carried out by means of a hierarchised, IRS–based[1] modal reduction in order to represent its eigenbehaviour as realistic as possible and to fulfil the requirement of low computational costs by reducing the number of degree of freedoms. Additionally, the journal bearing is considered by an online solution of the Reynolds equation, whereat the cavitation is handled by a transient acting, mass-conserving algorithm. This is based on the classical Elrod algorithm, but was extended by a regularisation, which enables a faster and more stable solution. Due to the general approach, both mechanical and tribological output quantities are accessible. This provides the possibility to draw a comparison with simpler approaches and to emphasize the benefit of the described procedure.

1 Introduction

The transient simulation of systems supported in journal bearings and exposed to high dynamic loads requires the description of the interaction between different field problems to determine the vibrations of the structure.

Firstly, the global behaviour due to the external loads has to be modelled including the elastic deformations. Taking large non-linear rigid body motions with superimposed small elastic deformations into account, an elastic MBS[2] approach based on the SID-formulation[3] is state of the art. To assure an adequate description of the transient behaviour, the hydrodynamic properties have to be considered.

In transient rotor-dynamics often a look-up table approach, which involves a stepwise linearisation of the bearing forces w.r.t. the displacements, is used in order to keep the numerical effort at a low level. Here it is not possible to represent the transient elastic deformations, which result from high dynamic forces. In contrast, a direct solution of the Reynolds equation is necessary yielding the actual hydrodynamic pressure in the fluid film. Whereas compressive loads are unproblematic for fluids, tensile loads lead to cavitational effects in the form of fluid vaporisation and emission of dissolved air. To consider these phenomena in the numerical scheme of EHL[4] analyses, several approaches exist. A pragmatical way is to postulate all negative pressure values to become zero, which is known as Half-Sommerfeld or Gümbel condition. The resulting drawback is the violation of the mass conservation, which was used to derive the Reynolds equation. Furthermore, differences concerning the minimal film thickness, the maximum pressure and especially the damping property can be expected.

Sophisticated approaches, which fulfil the mass conservation are given by Elrod's algorithm (Elrod and Adams (1974); Elrod (1981); Kumar and Booker (1991); Shi and Paranjpe (2002); Ausas et al. (2009)), the bi-phase model (Feng and Hahn (1986); Zeidan and Vance (1989); Tao et al. (2000); Glienicke et al. (2000)) as well as the ALE-approach[5] (Hu and Liu (1993); Martinet and Chabrand (2000); Boman and Ponthot (2004); Schweizer (2008)).

[1] Improved Reduction System
[2] Multibody System
[3] Standard Input Data
[4] Elasto-Hydrodynamic Lubrication
[5] Augmented-Lagrangian-Eulerian approach

The first one is widely-used also in EHL applications (Boedo et al. (1995); Shi and Paranjpe (2002); Rho and Kim (2003); Hajjam and Bonneau (2007)), whereat often the rotating structure is oversimplified to a mass point. Nevertheless – due to the necessarily fine discretisation of the cavitation boundary and the elastic structure on the bearing surface – high computational efforts arise. Aiming for stationary results, good solutions are achievable, whereas under dynamic conditions (depending on position, velocity, deformation and the numerical discretisation) cyclic repetitions of non-convergent iteration states during the solution of the Reynolds equation occur preventing a convergent pressure distribution in the fluid film.

As a consequence the time integration would fail, unless the solution strategy is able to assure a valid pressure distribution under all kinematic conditions. For that purpose a regularised variant of Elrod's algorithm was developed, which solves the problem by the introduction of a fuzzy cavitation state (Nitzschke et al. (2016)).

Using the example of a crank-drive and the support of the conrod's big end bearing, the differences between the Gümbel and the modified Elrod algorithm are discussed in the context of the numerical results and the necessary cpu-time. Beside the hydrodynamic properties, the increased level of detail concerning the film-fraction is also relevant for the interaction with further field problems, e.g. thermodynamics of the bearing and its surrounding.

2 Theoretical Principles

The main part of the presented approach is the implementation of the non-linear stiffness and damping properties of the bearing into the overall transient simulation. Starting with the numerical solution of the Reynolds equation using a regularised Elrod algorithm, the bearing reaction forces and torques are derived. Afterwards, the elastic behaviour of the bearing elements is taken into account via FEM[6]. Additionally, the global movement of the deformable components is modelled by an E-MBS[7] approach, which involves a model-reduction due to simulation time issues.

2.1 Hydrodynamics

2.1.1 Regularised Cavitation Approach

The pressure distribution in the fluid film of journal bearings due to the movement of shell and pin is described by the Reynolds PDE[8], which can be derived from Navier-Stokes equations and conservation of mass regarding the geometrical relations in the fluid gap. Elrod and Adams transformed this equation leading to the density relation $\theta = \varrho/\varrho_c$ as universal unknown, which depends on the compression modulus β

$$\underbrace{\frac{\partial}{\partial x}\left(\frac{h^3}{12\eta}\,g(\theta)\,\beta\,\frac{\partial\theta}{\partial x}\right)+\frac{\partial}{\partial y}\left(\frac{h^3}{12\eta}\,g(\theta)\,\beta\,\frac{\partial\theta}{\partial y}\right)}_{\text{Poiseuille-flow}}=\underbrace{\frac{U_\mathrm{S}+U_\mathrm{J}}{2}\,\frac{\partial(\theta\,h)}{\partial x}}_{\text{Couette-flow}}+\underbrace{\frac{\partial(\theta\,h)}{\partial t}}_{\text{squeeze-flow}}\quad . \tag{1}$$

As a result, the conservation of mass is ensured even in cavitating regions – i.e. in regions with divergent film height. This involves the implementation of a switch-function $g(\theta)$, which suppresses the Poiseuille-flow in these regions. The disadvantage of the resulting formulation is the calculation of the pressure from the film-fraction. Due to the magnitude of the compression modulus ($\beta \approx 10^9 Pa$), restrictive error tolerances for the film-fraction are needed to assure sufficient accuracy of pressure and thereby bearing forces as well as torques.

Utilising the fact that in the cavitation region a mixture of fluid and air occurs, Kumar and Booker introduced the application of the following approaches for density ϱ and viscosity η of the mixture depending on the film-fraction ϑ

$$\varrho = \vartheta\,\varrho_\mathrm{liq} + (1-\vartheta)\,\varrho_\mathrm{gas} \approx \vartheta\,\varrho_\mathrm{liq} \quad \text{and} \quad \eta = \vartheta\,\eta_\mathrm{liq} + (1-\vartheta)\,\eta_\mathrm{gas} \approx \vartheta\,\eta_\mathrm{liq} \tag{2}$$

[6] Finite Element Method
[7] Elastic Multibody System
[8] Partial Differential Equation

leading to a modified form of Eq. (1)

$$\frac{\partial}{\partial x}\left(\frac{\varrho_{\mathrm{liq}}\,h^3}{12\eta_{\mathrm{liq}}}\,\frac{\partial p}{\partial x}\right)+\frac{\partial}{\partial y}\left(\frac{\varrho_{\mathrm{liq}}\,h^3}{12\eta_{\mathrm{liq}}}\,\frac{\partial p}{\partial y}\right)=\frac{U_{\mathrm{S}}+U_{\mathrm{J}}}{2}\,\frac{\partial(\vartheta\,\varrho_{\mathrm{liq}}\,h)}{\partial x}+\frac{\partial(\vartheta\,\varrho_{\mathrm{liq}}\,h)}{\partial t}\quad . \tag{3}$$

This form is now depending on the pressure p as well as the film-fraction ϑ, which show a complementary relation. To obtain a solution, firstly the following relations are introduced in order to get a dimensionless formulation

$$H=\frac{h}{\Delta r^*},\ X=\frac{x}{r^*},\ Y=\frac{y}{r^*},\ \bar{\eta}=\frac{\eta_{\mathrm{liq}}}{\eta^*},\ u_m=\frac{U_{\mathrm{S}}+U_{\mathrm{J}}}{2},\ P=\frac{p\,(\Delta r^*)^2}{\eta^*\,|u_m|\,r^*},\ T=\frac{t\,|u_m|}{r^*}\quad . \tag{4}$$

Furthermore, the definition of a common variable Π is useful

$$\Pi(x,y)\overset{!}{=}\begin{cases}\vartheta(x,y)-1 & (x,y)\in\ \Omega_\vartheta\\ P(x,y) & (x,y)\in\ \Omega_p\end{cases}\quad , \tag{5}$$

which has to be interpreted depending on its actual value: In the pressure region Ω_p it correlates with the dimensionless pressure P, whereas in the cavitation region Ω_ϑ it contains the film-fraction. Defining a switch-function in analogy to Eq. (1)

$$g(\Pi)\overset{!}{=}\begin{cases}0 & \forall\,\Pi<0\\ 1 & \forall\,\Pi\geq 0\end{cases}\quad , \tag{6}$$

the equivalents to Eq. (5) and Eq. (6) read by reversal conclusions

$$\vartheta(x,y)=(1-g)\,(\Pi(x,y)+1)+g\quad \text{and} \tag{7}$$

$$P(x,y)=g\,\Pi(x,y)\quad , \tag{8}$$

which can be inserted in Eq. (3)

$$\begin{aligned}&\left[\frac{\partial}{\partial X}\left(\frac{H^3}{12\bar{\eta}}\,\frac{\partial(g\Pi)}{\partial X}\right)+\frac{\partial}{\partial Y}\left(\frac{H^3}{12\bar{\eta}}\,\frac{\partial(g\Pi)}{\partial Y}\right)-\mathrm{sgn}\,(u_m)\frac{\partial H}{\partial X}-\frac{\partial H}{\partial T}\right]\\ &+\left[\mathrm{sgn}\,(u_m)\frac{\partial\,((g-1)\Pi H)}{\partial X}+\frac{\partial\,((g-1)\Pi H)}{\partial T}\right]=0\quad .\end{aligned} \tag{9}$$

In order to solve Eq. (9) numerically, the bearing surface is dicretised using a FVM[9] approach. Therefore, in the pressure region central differences replace the differential quotient, whereas in the cavitation region due to the transport character of Couette-flow backward differences are applied. Finally, this leads to the non-linear system of equations

$$\mathbb{A}(g)\,\mathbb{p}=\mathbb{r}(g)\quad , \tag{10}$$

with a sparse, unsymmetric matrix $\mathbb{A}$ and a vector $\mathbb{p}$, which contains the unknown values of Π. The partition of the regions Ω_p and Ω_ϑ is initially unknown. Hence, Eq. (10) has to be solved by a fix-point iteration of the form

$$\mathbb{p}^{(i+1)}=\mathbb{A}(g^{(i)})^{-1}\,\mathbb{r}(g^{(i)})\quad . \tag{11}$$

A convergent state of iteration is found, if the values of the switch-function remain constant. Under transient loads the described algorithm tends to poor convergence, whereat cyclic repetitions in the solution of Eq. (11) occur. This behaviour complicates the application within rotor- or structuredynamic models. Obviously, in these cases the cavitational boundary is represented insufficiently, as its discretisation is coupled to the numerical grid. Therefore, a finer mesh is able to improve the situation, but the computational costs increase and the general problem remains: A given finite volume is either associated to the pressure *or* to the cavitation region. A redefinition of the Heaviside-like switch-function Eq. (6), e.g. by

$$g(\Pi)=\frac{1}{\pi}\,\arctan\left(\frac{\Pi}{1-\Pi^*}\right)+\frac{1}{2}\quad , \tag{12}$$

[9] Finite Volume Method

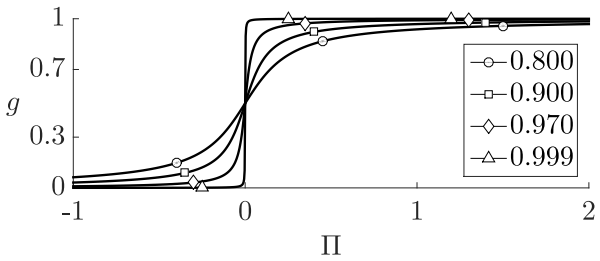

Figure 1: Influence of regularisation parameter Π^* on the smoothed switch-function Eq. (12).

allows a finite volume to be part of both regions. The stepwise respectivly discrete non-linearity of Eq. (10) is thereby regularised. Additionally, by the smooth transition a Newton-Raphson algorithm is applicable to solve the non-linear system of equations. For that purpose, Eq. (10) is to be seen as a function of $\mathbb{p}$

$$\mathbb{f}(\mathbb{p}) \mapsto \mathbb{r}(\mathbb{p}) - \mathbb{A}(\mathbb{p}) = 0 \quad , \tag{13}$$

whereof using a Taylor series interrupted after the first term yields

$$\mathbb{p}^{(i+1)} = \mathbb{p}^{(i)} - \mathbb{J}(\mathbb{p}^{(i)})^{-1}\, \mathbb{f}(\mathbb{p}^{(i)}) \tag{14}$$

with the Jacobian

$$\mathbb{J}(\mathbb{p}^{(i)}) = \left.\frac{\partial \mathbb{f}}{\partial \mathbb{p}}\right|_{\mathbb{p}^{(i)}} = \left.\frac{\partial \mathbb{r}}{\partial \mathbb{p}}\right|_{\mathbb{p}^{(i)}} - \left(\mathbb{A}(\mathbb{p}^{(i)}) + \left.\frac{\partial \mathbb{A}}{\partial \mathbb{p}}\right|_{\mathbb{p}^{(i)}} \mathbb{p}^{(i)}\right) \quad . \tag{15}$$

The partial derivatives of $\mathbb{r}$ and $\mathbb{A}$ can be expressed analytically and in addition only the derivative of Eq. (12) is required

$$\frac{\partial g}{\partial \Pi} = \left(\pi\,(1-\Pi^*)\left[1+\left(\frac{\Pi}{1-\Pi^*}\right)^2\right]\right)^{-1} \quad . \tag{16}$$

2.1.2 Validation of Hydrodynamics

The described approach was benchmarked in Nitzschke et al. (2016) against simulation results published in the literature Vijayaraghavan and Keith (1989) under static conditions. Furthermore, a convergence study was performed concerning the meshsize and the influence of the regularisation parameter Π^*. It was found, that from approximately 1000 unknowns and in the region of $\Pi^* = 0.9 \ldots 0.95$ the influences on the pressure distribution and the bearing force as well as its direction can be neglected.

Concerning dynamic loads, another example stated in Ausas et al. (2009) was used. Therein, a transient calculation of a single journal bearing under a load as it occurs in a main bearing of a crank-drive is examined. The equations of motion are restricted to a planar motion of the pin, which was modelled as a point mass. The shell features

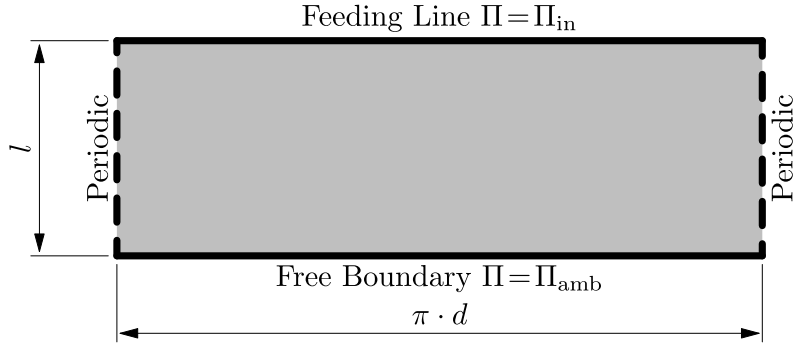

Figure 2: Scheme of half bearing surface with boundary conditions as stated in Ausas et al. (2009).

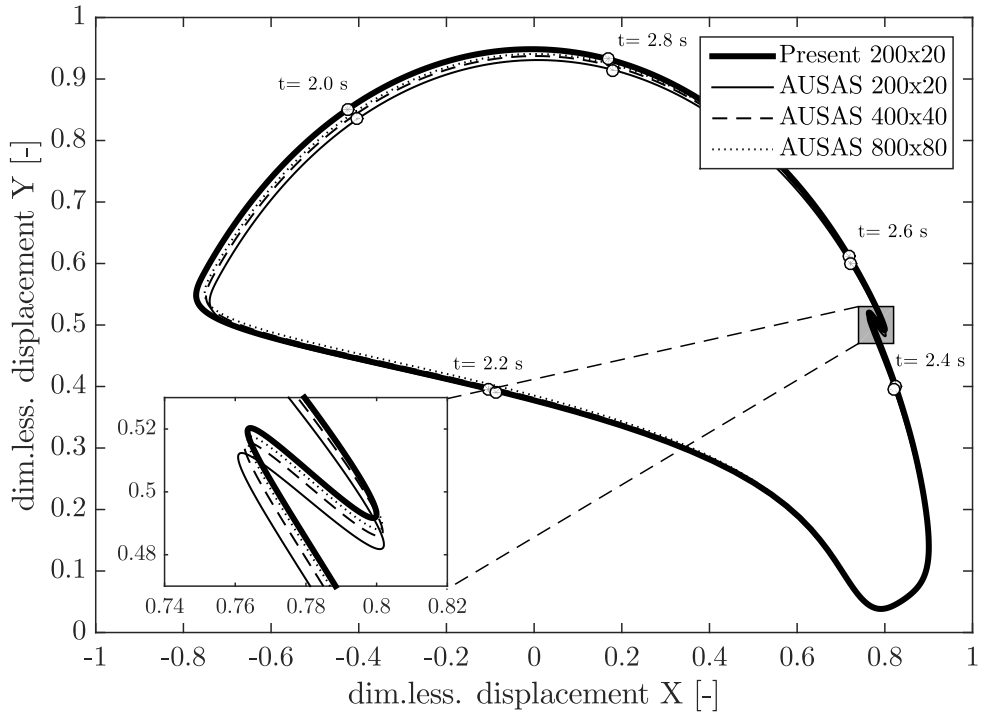

Figure 3: Orbit of the pin under transient conditions during one working cycle: comparison of the regularised algorithm against the classic algorithm of reference Ausas et al. (2009) with variation of the reference meshsize.

an axially centred circumferential groove ensuring the oil supply. Hence, only one bearing half is modelled, cf. Fig. 2.

As the reference solution and the corresponding source code is publicly available, the present approach can be opposed to the reference. The calculated orbits of the pin are displayed in Fig. 3 for one working cycle. In general, using an equal meshsize of 200x20, a good correlation between both approaches can be stated, whereat the reference tends to show the smaller orbit. It is interesting that, a refinement of the *reference mesh* leads to convergence against the 200x20 solution of the approach presented here. In reverse it can be concluded, that the latter shows a better solution quality even on a coarse mesh. This is caused by the property of Eq. (9) respectively Eq. (14) to allow grid point to be part of pressure as well as the cavitation region: The boundary between both is not longer restricted to run on the grid lines, but in contrast is able to cross a finite volume, cf. Fig. 4.

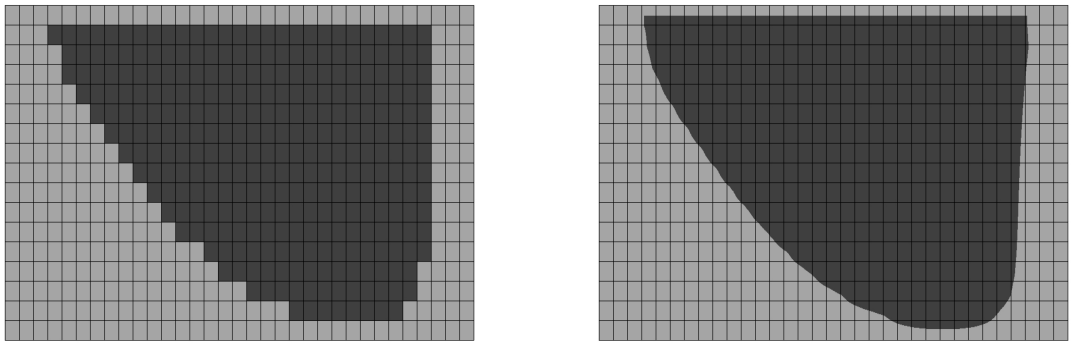

Figure 4: Representation of the boundary between pressure and cavitation region with the classic algorithm of reference (left) and the regularised algorithm (right) (Nitzschke et al. (2016)). The pressure region is indicated by light and the cavitation region by dark gray.

Table 1: Comparison of cpu-time under otherwise identical conditions concerning the results shown in Fig. 3.

regularised algorithm		**classic algorithm**	
meshsize	cpu-time [s]	meshsize	cpu-time [s]
200×20	254	200×20	480
		400×40	5790
		800×80	≈ 70000

Supplementary, due to the application of the Newton-Raphson algorithm the cpu-time is reduced by a factor of two under otherwise identical conditions. If the achieved accuracy is taken into account, the finest reference mesh has to be used for the comparison leading to a remarkable benefit of the regularised algorithm, cf. Tab. 1.

2.2 Elastic Deformations and Modal Reduction

Within the hydrodynamic contact in a crank shaft, the deformations in a conrod bearing show the same magnitude as the clearance. Hence, the elastic deformation of the bearing contour due to the mechanical loads and the appropriate surface velocity have to be taken into account. A proper method to provide the elastic behaviour during simulation is the FEM.

2.3 Structural Dynamics

2.3.1 FEM-approach of non-moving Structures

Starting from the Hamiltonian principle, according to discretisation and formulation of suitable shape functions of the variational function, a linear system of equations can be derived

$$\mathbb{M}\,\ddot{\mathbb{u}} + \mathbb{D}\,\dot{\mathbb{u}} + \mathbb{K}\,\mathbb{u} = \mathbb{f} \quad , \tag{17}$$

in which $\mathbb{M}$ represents the mass-, $\mathbb{D}$ the damping- and $\mathbb{K}$ the stiffness matrix. The vector $\mathbb{f}$ represents the external forces and $\mathbb{u}$ the displacements of nodal degrees of freedom. To minimise the numerical effort in the context of time integration algorithms, a reduction of the degree of freedoms is mandatory. This can be achieved by a reduction based on the master-slave concept or by a modal reduction.

2.3.2 Master-Slave Reduction

Firstly, the degrees of freedom of the overall structure are subdivided in master- and slave-degrees of freedom and sorted according to the following scheme

$$\begin{bmatrix} \mathbb{M}_{\mathrm{MM}} & \mathbb{M}_{\mathrm{MS}} \\ \mathbb{M}_{\mathrm{SM}} & \mathbb{M}_{\mathrm{SS}} \end{bmatrix} \begin{bmatrix} \ddot{\mathbb{u}}_{\mathrm{M}} \\ \ddot{\mathbb{u}}_{\mathrm{S}} \end{bmatrix} + \begin{bmatrix} \mathbb{D}_{\mathrm{MM}} & \mathbb{D}_{\mathrm{MS}} \\ \mathbb{D}_{\mathrm{SM}} & \mathbb{D}_{\mathrm{SS}} \end{bmatrix} \begin{bmatrix} \dot{\mathbb{u}}_{\mathrm{M}} \\ \dot{\mathbb{u}}_{\mathrm{S}} \end{bmatrix} + \begin{bmatrix} \mathbb{K}_{\mathrm{MM}} & \mathbb{K}_{\mathrm{MS}} \\ \mathbb{K}_{\mathrm{SM}} & \mathbb{K}_{\mathrm{SS}} \end{bmatrix} \begin{bmatrix} \mathbb{u}_{\mathrm{M}} \\ \mathbb{u}_{\mathrm{S}} \end{bmatrix} = \begin{bmatrix} \mathbb{f}_{\mathrm{M}} \\ \mathbb{f}_{\mathrm{S}} \end{bmatrix} \quad , \tag{18}$$

whereat the master-group is still present after the reduction and the slave-group will be expressed as a function of the master degrees of freedom using a suitable transformation matrix $\mathbb{Q}_{red}$

$$\begin{bmatrix} \mathbb{u}_{\mathrm{M}} \\ \mathbb{u}_{\mathrm{S}} \end{bmatrix} = \mathbb{Q}_{\mathrm{red}}\,\mathbb{u}_{\mathrm{M}} \quad . \tag{19}$$

Different variants with specific advantages and disadvantages exist: The simplest form of reduction dates back to Guyan (1965) and neglects all dynamic effects of the slave structure, which is widely known as static condensation

$$\begin{bmatrix} \mathbb{u}_{\mathrm{M}} \\ \mathbb{u}_{\mathrm{S}} \end{bmatrix} = \begin{bmatrix} \mathbb{I} \\ -\mathbb{K}_{\mathrm{SS}}^{-1}\,\mathbb{K}_{\mathrm{MS}}^{T} \end{bmatrix} \mathbb{u}_{\mathrm{M}} = \mathbb{Q}_{\mathrm{G}}\,\mathbb{u}_{\mathrm{M}} \quad . \tag{20}$$

The application of the transformation matrix to all system matrices and the subsequent symmetrisation

$$\mathbb{S}_{\mathrm{G}} = \mathbb{Q}_{\mathrm{G}}^{T}\, \mathbb{S}\, \mathbb{Q}_{\mathrm{G}} \qquad \text{with} \qquad \mathbb{S} = \mathbb{M},\, \mathbb{D},\, \mathbb{K} \tag{21}$$

leads to the differential equation of the reduced system

$$\mathbb{M}_{\mathrm{G}}\, \ddot{\mathfrak{u}}_{\mathrm{M}} + \mathbb{D}_{\mathrm{G}}\, \dot{\mathfrak{u}}_{\mathrm{M}} + \mathbb{K}_{\mathrm{G}}\, \mathfrak{u}_{\mathrm{M}} = \mathfrak{f}_{\mathrm{G}} \quad . \tag{22}$$

However, as the excitation frequency rises, increasing deviations occur compared to the dynamic behaviour of the unreduced structure. An improvement can be made by consideration of the dynamic behaviour of the slave degrees of freedom. A popular method of improvement without the usage of additional modal degrees of freedom (as done in the Craig-Bampton- (Craig (2000)) or the SEREP-reduction (O'Callahan (1989b))) is the IRS-method by O'Callahan (1989a). Therein, the Guyan approach is extended with pseudostatic inertial forces, which leads after some conversions to the following transformation matrix

$$\begin{bmatrix} \mathfrak{u}_{\mathrm{M}} \\ \mathfrak{u}_{\mathrm{S}} \end{bmatrix} = \mathbb{Q}_{\mathrm{IRS}}\, \mathfrak{u}_{\mathrm{M}} = \left(\mathbb{Q}_{\mathrm{G}} + \mathbb{P}\, \mathbb{M}\, \mathbb{Q}_{\mathrm{G}}\, \mathbb{M}_{\mathrm{G}}^{-1}\, \mathbb{K}_{\mathrm{G}}\right) \mathfrak{u}_{\mathrm{M}} \qquad \text{with} \qquad \mathbb{P} = \begin{bmatrix} 0 & 0 \\ 0 & \mathbb{K}_{\mathrm{SS}}^{-1} \end{bmatrix} \quad . \tag{23}$$

The procedure can be extended iteratively (O'Callahan (1989b)), whereby the eigenfrequencies of the reduced system are converging to that of the unreduced system

$$\mathbb{Q}_{\mathrm{IRS},i+1} = \mathbb{Q}_{\mathrm{G}} + \mathbb{P}\, \mathbb{M}\, \mathbb{Q}_{\mathrm{IRS},i}\, \mathbb{M}_{\mathrm{IRS},i}^{-1}\, \mathbb{K}_{\mathrm{IRS},i} \quad . \tag{24}$$

However, the drawback of this iteration is an increasing condition of the system matrices. Hence, it has to be terminated after reaching a sufficient accuracy or exceeding a critical condition number.

2.3.3 Modal Reduction

Alternatively, the reduction can be based on the eigenvectors. The homogeneous solution of the boundary value problem consists of the n_k eigenfrequencies ω_k and the corresponding eigenvectors $\hat{\mathfrak{u}}_k$

$$\left[\mathbb{K}_{\mathrm{red}} - (\omega_k)^2\, \mathbb{M}_{\mathrm{red}}\right]\, \hat{\mathfrak{u}}_k = 0 \quad . \tag{25}$$

This results in a transition from the physical coordinates $\mathfrak{u}$ to the modal coordinates $\mathfrak{q} = [q_1 \dots q_k]$

$$\mathbb{M}_{\mathrm{red}}\, \ddot{\mathfrak{u}} + \mathbb{D}_{\mathrm{red}}\, \dot{\mathfrak{u}} + \mathbb{K}_{\mathrm{red}}\, \mathfrak{u} \quad = \mathfrak{f}_{\mathrm{red}} \quad \Rightarrow \tag{26}$$

$$\mathbb{M}_{\mathrm{mod}}\, \ddot{\mathfrak{q}} + \mathbb{D}_{\mathrm{mod}}\, \dot{\mathfrak{q}} + \mathbb{K}_{\mathrm{mod}}\, \mathfrak{q} = \mathfrak{f}_{\mathrm{mod}} \tag{27}$$

using the transformation

$$\mathfrak{u} = \mathbb{Q}_{\mathrm{mod}}\, \mathfrak{q} = \hat{\mathbb{U}}\, \mathfrak{q} \qquad \text{with} \quad \hat{\mathbb{U}} = [\hat{\mathfrak{u}}_1 \dots \hat{\mathfrak{u}}_k] \quad . \tag{28}$$

This transformation is initially exact and it can be shown that each deformation state can be represented as the superposition of different eigenvectors.

The reduction is achieved by eliminating those eigenvectors $\hat{\mathfrak{u}}_j$ of the modal matrix $\hat{\mathbb{U}}$ which – due to the frequency spectrum of the external loads – result in modal amplitudes q_j with insignificant magnitude (Dietz (1999)). These are predominantly high-frequency components of the deformation, which in addition usually show a strong damping.

2.4 Elastic Multi Body Dynamics

For the application example of the crank drive, the individual components are subject to large rigid body movements, on which small elastic deformations are superimposed. With this background, the use of a FEM description, which would inevitably have to be geometrically non-linear, is numerically very complex. For this reason, elastic multi-body algorithms are preferred which have been specifically developed with this focus using the floating-frame-of-reference approach.

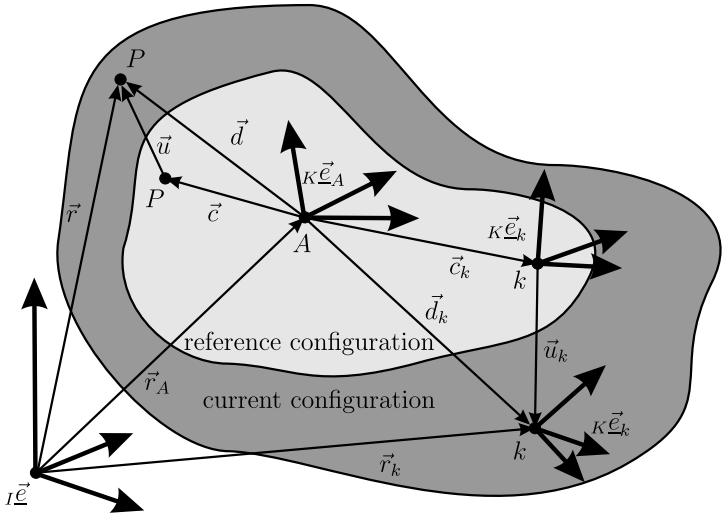

Figure 5: Representation of the position vector $\mathbb{r}$ in initial- and deformed configuration and its segmentation in rigid body part $\mathbb{c}$ as well as the elastic deformation $\mathbb{u}$ according to Woschke (2013).

As a starting point for their description, the integral over the difference of the variations of the internal and the kinetic energy can be used, which must be in equilibrium with the virtual work of the external loads, consisting of volume- and single-forces

$$\begin{aligned} 0 &\equiv \int_{t_1}^{t_2} \left(\delta E_{\text{kin}} - \delta E_{\text{in}} + \delta W\right)\, dt \\ &= \int_{t_1}^{t_2} \left(\int_V \delta\dot{\mathbb{r}}^T\, \dot{\mathbb{r}}\, \rho\, dV - \int_V \delta\varepsilon^T\, \sigma\, dV + \int_{V^s} \delta\mathbb{r}^T\, \mathbb{s}^v\, dV + \sum_i \left(\delta\mathbb{r}_i^T\, \mathbb{F}_i\right) \right) dt \quad . \end{aligned} \tag{29}$$

Using the fundamental lemma and the fact that the variation vanishes at the times t_1 and t_2 yields

$$0 \equiv \underbrace{\int_V \delta\mathbb{r}^T\, \ddot{\mathbb{r}}\, \rho\, dV}_{\text{inertia effects}} + \underbrace{\int_V \delta\varepsilon(\mathbb{u})^T\, \sigma(\mathbb{u})\, dV}_{\text{inner forces}} - \underbrace{\left[\int_{V^s} \delta\mathbb{r}^T\, \mathbb{s}^v\, dV + \sum_i \left(\delta\mathbb{r}_i^T\, \mathbb{f}_i\right) \right]}_{\text{external loads}} \quad . \tag{30}$$

The equation of motion now contains volume integrals with non-linear dependence on location and time. If, at the same time, the elastic deformation $\mathbb{u}$ is replaced by the modal coordinates $\mathbb{q}$ by utilising the described reduction methods, the following relationships according to Fig. 5 are obtained

$$\begin{aligned} \mathbb{r} &= \mathbb{Q}_{IK\,K}(\mathbb{r}_A + \mathbb{c} + \mathbb{u}) = \mathbb{Q}_{IK\,K}\Big(\mathbb{r}_A + \mathbb{c} + \hat{\mathbb{U}}\mathbb{q}\Big) \quad , \\ \ddot{\mathbb{r}} &= \mathbb{Q}_{IK\,K}\Big(\ddot{\mathbb{r}}_A + \Big(\mathbb{c} + \hat{\mathbb{U}}\mathbb{q}\Big)^T \times \dot{\mathbb{w}} + \hat{\mathbb{U}}\ddot{\mathbb{q}} + 2\mathbb{w} \times \hat{\mathbb{U}}\dot{\mathbb{q}} + \mathbb{w} \times \Big(\mathbb{w} \times \big(\mathbb{c} + \hat{\mathbb{U}}\mathbb{q}\big)\Big)\Big) \quad , \\ \delta\mathbb{r} &= \mathbb{Q}_{IK\,K}\Big(\delta\mathbb{r}_A + \delta\mathbb{w} \times \mathbb{r}_A + \Big(\mathbb{c} + \hat{\mathbb{U}}\mathbb{q}\Big) \times \delta\mathbb{w} + \hat{\mathbb{U}}\delta\mathbb{q}\Big) \quad . \end{aligned} \tag{31}$$

Thereby, all terms are expressed as a function of the angular velocity $\mathbb{w}$ as well as the modal coordinates $\mathbb{q}$ and their derivatives $\dot{\mathbb{q}}$, which leads to a formulation of Eq. (30) in the form of

$$\mathbb{M}_{\text{MBS}}(\mathbb{q})\, \mathbb{a} \quad + \quad \mathbb{h}_\omega(\mathbb{w}, \mathbb{q}, \dot{\mathbb{q}}) + \mathbb{h}_{\text{el}}(\mathbb{q}, \dot{\mathbb{q}}) = \mathbb{h}_{\text{o}}(\mathbb{q}) \quad \text{mit} \quad \mathbb{a} = \begin{bmatrix} \ddot{\mathbb{r}}_A \\ \dot{\mathbb{w}} \\ \ddot{\mathbb{q}} \end{bmatrix} \quad . \tag{32}$$

The modal reduction is an integral part of the implementation of elastic bodies into MBS applications. Due to the orthogonality properties, they allow a decoupling of the equation of motions into n linearly independent differential equations. At the same time, a master-slave reduction can be pre-set to the modal reduction, in order to limit the

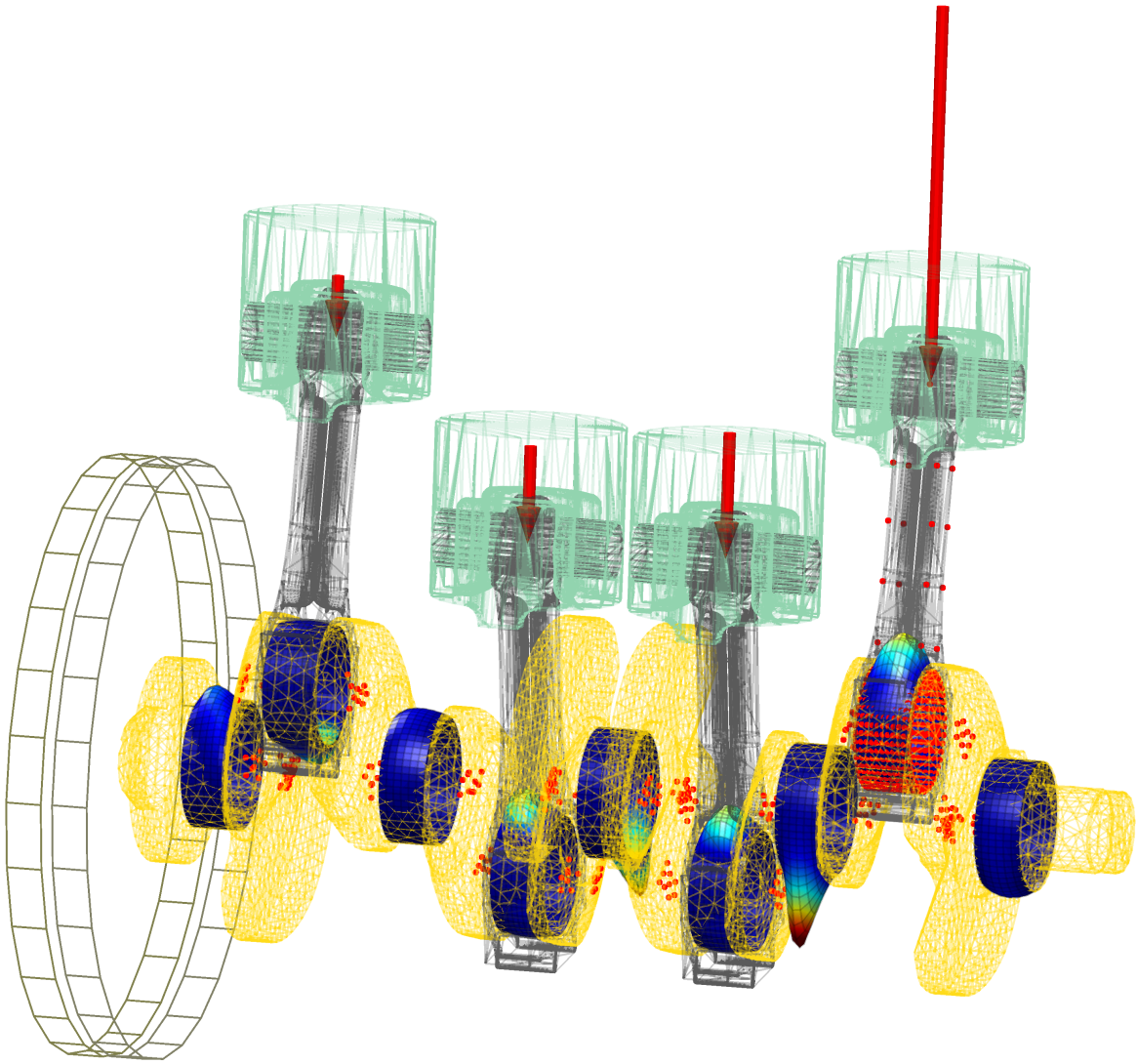

Figure 6: Model of the crankdrive with elastic crankshaft and elastic conrod on cylinder 1 (C_1) shortly after TDC[10]of C_1. The dots indicate the markers resulting from the master degree of freedoms. In addition, the lubrication film pressures are visualised on the main bearings and on the conrod's big end bearings. The arrows on the pistons represent the forces due to the gas pressure in the cylinders.

eigenvectors to the information essential for the deformation description. This results in the following substitution

$$\mathbb{u} = \mathbb{Q}_{\text{IRS}}\mathbb{u}_{\text{M}} = \mathbb{Q}_{\text{IRS}}\hat{\mathbb{U}}\mathbb{q} \quad , \tag{33}$$

which can be applied in Eq. (31) instead of the straight modal reduction.

3 Model

The combination of the described approaches with regard to hydrodynamics and elastic multi-body simulation is demonstrated by means of a conrod big end bearing of a crankdrive, cf. Fig. 6.

Conrod For this purpose, the conrod is first discretised by finite elements and then reduced to 1503 degrees of freedom using the described IRS-based master-slave approach. The master nodes are arranged on the one hand uniformly over the shank of the conrod and, on the other hand, are concentrated in the bearing shell in order to be

[10]Top Dead Centre

able to accurately represent the deformation in the fluid gap. The distribution of the nodes is coupled to the mesh required for the hydrodynamics, in order to avoid interpolation of the deformations and the associated velocities. Subsequently, a modal reduction is used, in order to achieve decoupling of the equations of motion. The eigenforms to be considered depend primarily on the excitation frequency spectrum. But in addition, special eigenforms have to be taken into account to inclose the local deformations in the bearing shell. These deformations are described by eigenforms whose natural frequency is clearly above each frequency contained in the load spectrum. In this case, the influence of the deformation on the pressure build-up in the journal bearing and thus in the loads is decisive, whereat a renouncement of the corresponding eigenforms results in exaggerated hydrodynamic pressures. The decisive point of the modal reduction is thus given by the selection of the eigenforms used to describe the deformation.

Neglecting the effect of all inertia forces and influences from damping compared to those from stiffness, the equation of motion of a modal reduced elastic body Eq. (26) can be formulated by

$$\mathbb{M}_{\text{mod}}\,\ddot{\mathfrak{q}} + \mathbb{D}_{\text{mod}}\,\dot{\mathfrak{q}} \ll \mathbb{K}_{\text{mod}}\,\mathfrak{q} \quad \rightsquigarrow \quad \mathbb{K}_{\text{mod}}\,\mathfrak{q} = \mathbb{f}_{\text{mod}} \quad . \tag{34}$$

This assumption applies formally only to slowly moving elastic bodies, taking into account a low attenuation as well as a low rate of change concerning the external loads. However, the results obtained are also applicable to dynamically loaded systems in the context of journal bearing simulation because the local deformations primarily result from the acting external loads and the deformation rate remains moderate.

Assuming that the forces acting on the structure are known, the modal deformations q_i can be determined. If they are weighted with regard to their share in the overall deformation state using the modal participation factor

$$\text{MPF}_i = \frac{|q_i|}{\sum\limits_i |q_i|} \cdot 100\% \quad , \tag{35}$$

an explicit selection of significant eigenforms can be achieved. Also a set of load collectives – e.g. obtained from dynamic simulations – can be considered by superposition of significant eigenforms of each load step.

For the knowledge of the external loads of the deformed model, formally a complete simulation with a high number of modal state variables is necessary. However, it could be shown that the general trend of hydrodynamic loads using a simulation with a rigid bearing shell is similar to an elastic one. Hence, the hydrodynamic loads of a rigid calculation – wich are obtainable with a lower numerical effort – can be used as input data for the selection of the participating eigenvectors.

The minimal percentage contribution to the deformation, which must be taken into account, is not comprehensively algorithmic, but is always associated with the actual load case. Further details concerning the choice of eigenforms are shown in Woschke (2013), Woschke et al. (2007) and Wallrapp (1999). For the conrod considered here, 74 suitable eigenforms from the first 200 eigenforms were selected and taken into account for the calculation.

Depending on the algorithm used for the master-slave reduction, deviations of the eigenfrequencies between reduced and unreduced structure result. These are summarised in Tab. 2 using the example of the lowest and highest natural frequency selected for the deformation. The reduction methods consistently predicate a stiffer behavior than is represented by the unreduced structure, whereat the differences increase as the order of the eigenfrequencies increases. The deviations are greatest in the Guyan reduction due to the disregarded dynamic properties of the slave structure. The IRS reduction converges with increasing number of iterations monotonously against the values of the unreduced model. The highest eigenfrequency to be considered defines the numerical stiffness of the resulting differential equation system and thus represents an important indicator for time integration with respect to the maximum step size.

Table 2: Influence on the conrod's eigenfrequencies due to the master-slave-reduction method

method	**1st EF [Hz]**	...	**188th EF [kHz]**	**rel. deviation to unreduced [%]**
unreduced	2058	...	120.9	-
Guyan	2063	...	262.1	117
IRS (5 iterations)	2063	...	134.7	11
IRS (10 iterations)	2063	...	123.0	2

Crank shaft The local deformations at the bearing area in radial direction are negligibly small on the crankshaft due to the solidly designed pins on the main and conrod bearings. However, in the course of the ignition sequence of the individual cylinders, a time delay concerning the introduction of the gas forces occurs leading to a global deformation. Subsequently, the crankshaft is also reduced by the described methods. The selection of the master nodes was made with a restriction on the degrees of freedom required for the force application into the bearing points. For this purpose, the bearing pin surfaces were assumed to be non-deformable and rigidly connected to a master node, which is central with respect to the pin – nine nodes remain after reduction. According to the highest frequency contained in the excitation, the consideration of the 13 first eigenforms is sufficient here.

4 Results

In this section, the results concerning the big end bearing of the conrod are discussed depending on different modelling approaches of MBS and hydrodynamics, cf. Tab. 3.

Table 3: Modelling approaches

variant	label	description MBS	description hydrodynamics
a)	$\mathrm{CR}_{\mathrm{el}} + \mathrm{HD}_{\mathrm{reg/reg}}$	conrod as well as crankshaft elastic	conrod bearing and main bearings with regularised cavitation algorithm
b)	$\mathrm{CR}_{\mathrm{el}} + \mathrm{HD}_{\mathrm{reg/spring}}$	conrod as well as crankshaft elastic	conrod bearing with regularised cavitation algorithm, main bearings with isotropic spring-damper elements
c)	$\mathrm{CR}_{\mathrm{el}} + \mathrm{HD}_{\mathrm{gue/spring}}$	conrod as well as crankshaft elastic	conrod bearing with Gümbel cavitation algorithm, main bearings with isotropic spring-damper elements
d)	$\mathrm{CR}_{\mathrm{rig}} + \mathrm{HD}_{\mathrm{reg/spring}}$	conrod rigid, crankshaft elastic	conrod bearing with regularised cavitation algorithm, main bearings with isotropic spring-damper elements
e)	$\mathrm{CR}_{\mathrm{rig}} + \mathrm{HD}_{\mathrm{gue/spring}}$	conrod rigid, crankshaft elastic	conrod bearing with Gümbel cavitation algorithm, main bearings with isotropic spring-damper elements

Due to the transient load, the elastic deformation and the associated surface velocity are varying during the working cycle and influence the hydrodynamic film thickness and its derivative w.r.t. time, further details can be found in Daniel (2013). As a consequence of the online approach for solving the Reynolds equation, the pressure distribution and the resulting bearing reactions can be analysed. Additionally, due to the mass-conserving cavitation algorithm, the transient development of the film-fraction ϑ is accessible. The mentioned quantities are displayed exemplarily at the TDC in Fig. 7: The radial deformation of the bearing surface is dominated by a global ovalisation due to inertia forces, which is superimposed by local deformations in the region of maximum hydrodynamic pressure. The gap function consist of the radial deformation plus the gap due to the rigid body kinematics. As a consequence, the maximum pressure arises in the region with minimal gap. The pressure build-up is also influenced by the transient film-fraction – only in regions with sufficient fluid filling pressure values above the cavitation pressure can occur. Furthermore, in the visualisation of the film-fraction the oil-supply is noticeable.

The evaluation of these quantities for every time step of a complete working cycle is not practicable at this point, therefore integral quantities like the orbit of the crankpin w.r.t. the conrod's big end as well as the maximum pressure and the minimal film thickness are discussed in correlation to the modelling approaches, cf. Tab. 3.

The orbit is displayed normalised relative to the bearing clearance. Firstly, in Fig. 8 the different parts of the orbit are assigned to the four strokes of cylinder 1. In particular, during compression and power stroke sharp peaks occur in the orbit, which result from the changing gas force due to the pressure in the combustion chamber. Basically, Fig. 9 shows the evident difference between the elastic and the rigid modelling of the conrod. Due to the elastic deformation values of the normalised total displacement $v_{\text{total}} = \sqrt{v_x^2 + v_y^2} > 1$ occur.

Both, the elastic as well as the rigid results show a significant deviation in the utilisation of the clearance concerning the modelling of the cavitation algorithm. The regularised Elrod algorithm tends to larger displacements caused by the delayed pressure build-up as a result of the film-fraction's transient development. In contrast, the Gümbel approach leads, apparently due to the violation of mass conservation, to larger reserves before solid contact occurs.

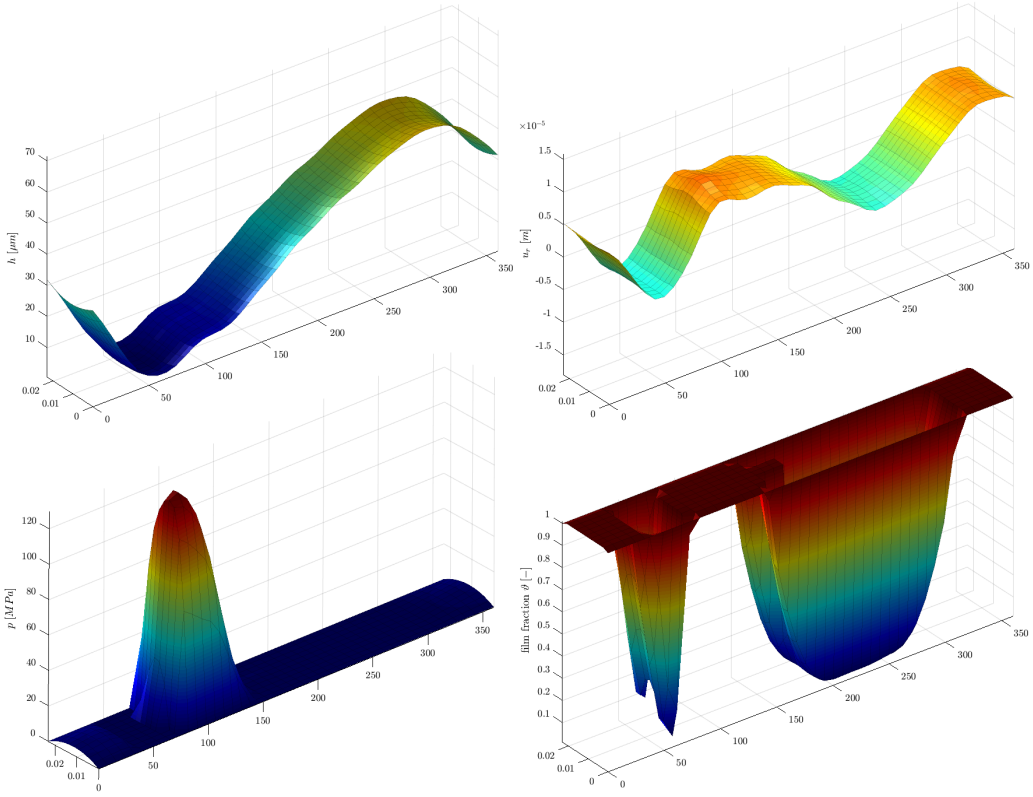

Figure 7: Input and result field-quantities of Reynolds equation at TDC: gap function (top left), radial deformation of bearing surface (top right), pressure (bottom left), film-fraction (bottom right).

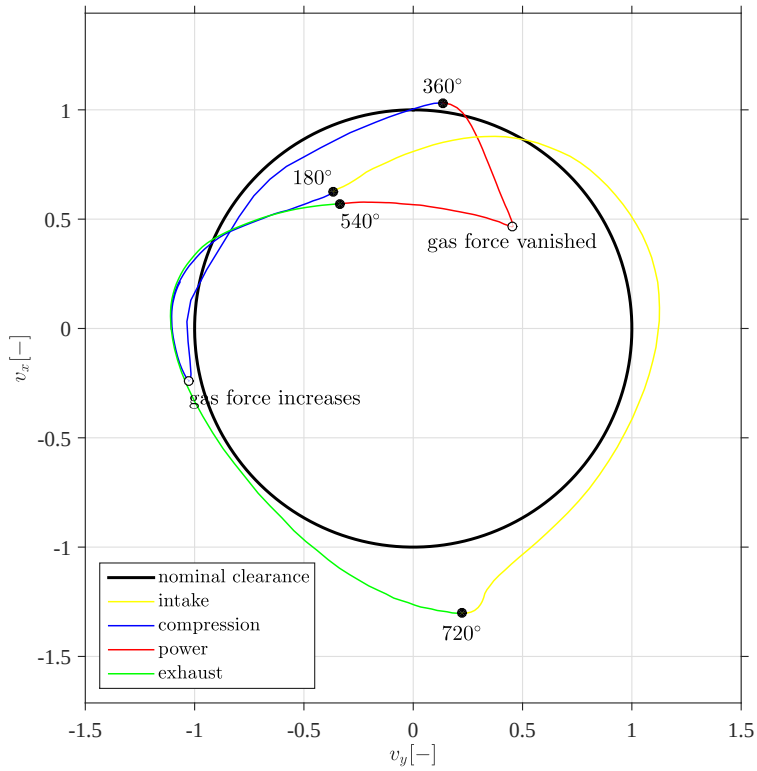

Figure 8: Orbit of crank pin w.r.t. the conrod's big end: correlation to the four strokes of the working cycle.

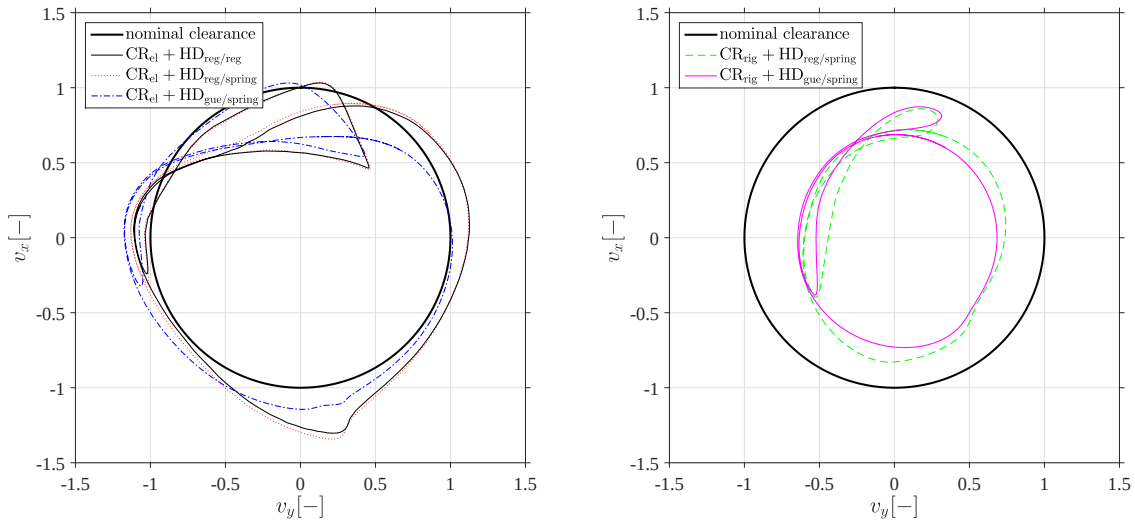

Figure 9: Orbit of crank pin w.r.t. the conrod's big end using different modelling approaches: elastic conrod (left), rigid conrod (right). Additionally, the nominal clearance is displayed as a bold line, which visualises the undeformed contour.

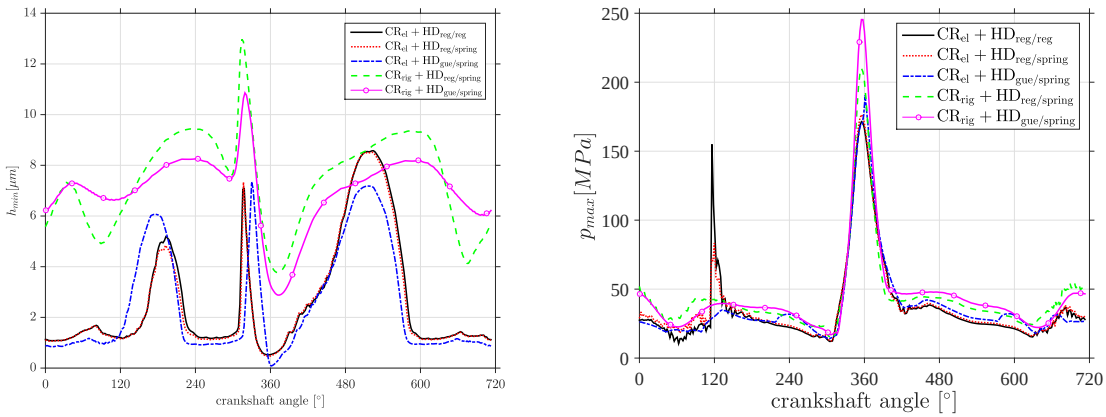

Figure 10: Tribological quantities during a working cycle: minimal film thickness (left) and maximum pressure (right).

With regard to the influence of the main bearings and the remaining conrod bearings on the crankpin orbit, only slightly differences occur, which hardly legitimate the extended effort.

Concluding, the minimal film thickness and the maximum hydrodynamic pressure are investigated as tribological indicators of the bearing's operating grade, cf. Fig. 10 left. Contrarily to the crankpin orbit, which is meaningful only at the bearing mid, here the film thickness is evaluated in the whole bearing, whereby potential wear on the bearing's edges due to tilting of the bearing surfaces can be identified. But coinciding with the results obtained on the crankpin orbit, the influence of tilting is negligeble in the present case.

The maximum pressure in the fluid film shows in wide ranges of the working cycle only minor differences between the modelling approaches, cf. Fig. 10 right. Merely on TDC a decrease can be observed with increasing modelling grade. This behaviour is caused by the increasing compliance due to elasticity of the conrod, which results in an enlargement of the load zone. This trend is amplified by the cavitation as the partly filled fluid gap leads to a softer bearing reaction resulting in lower pressure values.

Referring to the tribological quantities, the modelling of the remaining bearings is also of minor importance.

5 Summary and Outlook

The paper at hand shows exemplarily the implementation of dynamic loaded components or systems supported in journal bearings into a holistic MBS-based simulation. Therein, the level of detail concerning the hydrodynamics is extended by introducing a regularised Elrod–algorithm, which is compared to existing simplified approaches. Firstly, a significant deviation from these assumptions can be shown, which e.g. results in smaller minimal film thickness preventing an overestimation of carrying reserves. Furthermore, a significant advantage in cpu-time of the new approach appeared compared to the classic Elrod–algorithm. It can also be concluded, that the modelling depth of adjacent bearings has only a small impact on the bearing on the investigated conrod.

The presented approach can be transferred in a similar manner to other tribological contacts (axial or floating ring bearings) and cavitation models (bi-phase-model). Regarding the floating ring bearing appropriate results are published in Nitzschke (2016). In addition to the improved model quality, a basis for the integration of the thermal field problem is given through the mass-preserving cavitation algorithm, because the transient gap filling is required as an input of the energy equation, as mentioned in Woschke (2013).

Acknowledgment

The results were generated in the framework of the project WO 2085/2 ”Numerische Analyse des transienten Verhaltens dynamisch belasteter Rotorsysteme in Gleit- und Schwimmbuchsenlagern unter Berücksichtigung kavitativer Effekte”, which is supported by the DFG. This support is gratefully acknowledged.

References

Ausas, R. F.; Jai, M.; Buscaglia, G. C.: A mass-conserving algorithm for dynamical lubrication problems with cavitation. *Journal of Tribology*, 131, 3, (2009), 031702–031702.

Boedo, S.; Booker, J.; Wilkie, M.: A mass conserving modal analysis for elastohydrodynamic lubrication. *Tribology Series*, 30, (1995), 513–523.

Boman, R.; Ponthot, J.-P.: Finite element simulation of lubricated contact in rolling using the arbitrary lagrangian–eulerian formulation. *Comput. Methods Appl. Mech. Engrg.*, 193, (2004), 4323–4353.

Craig, R. R.: Coupling of substructures for dynamic analysis: An overwiew. *AIAA Journal*, 41.

Daniel, C.: *Simulation von gleit-und wälzgelagerten Systemen auf Basis eines Mehrkörpersystems für rotordynamische Anwendungen*. Ph.D. thesis, Magdeburg, Universität, (2013).

Dietz, S.: *Vibration and Fatigue of Vehicle Systems Using Component Modes*. Ph.D. thesis, Technische Universität Berlin (1999).

Elrod, H. G.: A cavitation algorithm. *Journal of Tribology*, 103, 3, (1981), 350–354.

Elrod, H. G.; Adams, M. L.: A computer program for cavitation and starvation problems. In: D. Dowson; M. Godet; C. Taylor, eds., *Cavitation and related phenomena in lubrication (Proc. 1st Leeds-Lyon Symposium on Tribology, Leeds, England)*, pages 37–41, Mechanical Engineering Publications (1974).

Feng, N. S.; Hahn, E. J.: Density and viscosity models for two-phase homogeneous hydrodynamic damper fluids. *A S L E Transactions*, 29, 3, (1986), 361–369.

Glienicke, J.; Fuchs, A.; Peng, D.; Lutz, M.; Freytag, C.: Robuste Lagerungen. Abschlussbericht Vorhaben 662 Heft 694, FVV (2000).

Guyan, R. J.: Reduction of stiffness and mass matrices. *AIAA Journal*, 3, 2, (1965), 380.

Hajjam, M.; Bonneau, D.: A transient finite element cavitation algorithm with application to radial lip seals. *Tribology International*, 40, (2007), 1258–1269.

Hu, Y.-K.; Liu, W. K.: An ale hydrodynamic lubrication finite element method with application to strip rolling. *International Journal for Numerical Methods in Engineering*, 36, (1993), 855–880.

Kumar, A.; Booker, J. F.: A finite element cavitation algorithm. *Journal of Tribology*, 113, 2, (1991), 279–284.

Martinet, F.; Chabrand, P.: Application of ale finite elements method to a lubricated friction model in sheet metal forming. *International Journal of Solids and Structures*, 37, (2000), 4005–4031.

Nitzschke, S.: *Instationäres Verhalten schwimmbuchsengelagerter Rotoren unter Berücksichtigung masseerhaltender Kavitation*. Ph.D. thesis, Otto-von-Guericke Universität Magdeburg (2016).

Nitzschke, S.; Woschke, E.; Schmicker, D.; Strackeljan, J.: Regularised cavitation algorithm for use in transient rotordynamic analysis. *International Journal of Mechanical Sciences*, 113, (2016), 175–183.

O'Callahan, J.: A procedure for an improved reduced system (irs). *Proceedings of the 7th International Modal analysis conference, Society of Experimental Mechanics*, 7, (1989a), 17 – 21.

O'Callahan, J.: System equivalent reduction and expansion process. *Proceedings of the 7th International Modal analysis conference, Society of Experimental Mechanics*, 7, (1989b), 29 – 37.

Rho, B.-H. R.; Kim, K.-W.: Acoustical properties of hydrodynamic journal bearings. *Tribology International*, 36, (2003), 61–66.

Schweizer, B.: Ale formulation of reynolds fluid film equation. *ZAMM*, 88, 9, (2008), 716–728.

Shi, F.; Paranjpe, R.: An implicit finite element cavitation algorithm. *Computer modeling in engineering and sciences*, 3, 4, (2002), 507–516.

Tao, L.; Diaz, S.; San Andres, L.; Rajagopal, K.: Analysis of squeeze film dampers operating with bubbly lubricants. *Journal of tribology*, 122, 1, (2000), 205–210.

Vijayaraghavan, D.; Keith, T. G.: Development and evaluation of a cavitation algorithm. *Tribology Transactions*, 32, 2, (1989), 225–233.

Wallrapp, S. M., O.; Wiedemann: Multibody system simulation of deployment of a flexible solar array. In: *4th International Conference on Dynamics and Control of Structures in Space* (1999).

Woschke, E.: *Simulation gleitgelagerter Systeme in Mehrkörperprogrammen unter Berücksichtigung mechanischer und thermischer Deformationen*. Dissertation, Otto-von-Guericke-Universität Magdeburg (2013).

Woschke, E.; Daniel, C.; Strackeljan, J.: Reduktion elastischer Strukturen für MKS Anwendungen. In: *Tagungsband 8. Magdeburger Maschinenbau-Tage* (2007).

Zeidan, F. Y.; Vance, J. M.: Cavitation leading to a two phase fluid in a squeeze film damper. *Tribology Transactions*, 32, 1, (1989), 100–104.

Address: S. Nitzschke, E. Woschke , C. Daniel,
IFME, Otto-von-Guericke-Universität Magdeburg, Universitätsplatz 2, 39106 Magdeburg, Deutschland
email: {steffen.nitzschke,elmar.woschke,christian.daniel}@ovgu.de